J Petrol Explor Prod Technol (2014) 4:215–231
DOI 10.1007/s13202-013-0088-4

ORIGINAL PAPER - PRODUCTION GEOPHYSICS

Integrated approach to geopressure detection in the X-field, Onshore Niger Delta

Sylvester A. Ugwu · Cyril N. Nwankwo

Received: 3 August 2013 / Accepted: 19 October 2013 / Published online: 9 November 2013

Abstract Geopressured sedimentary formations are common within the more prolific deeper hydrocarbon reserves in the Niger Delta basin. While overpressured zones could serve as tools for hydrocarbon prospectivity evaluation, they are significant safety concern during drilling. Post-drill pore pressure prediction using wireline log and mudlog was carried out in the X-field, Onshore Niger Delta basin to predict the depth of abnormal pressure occurrence, estimate the amount of pore pressure encountered and its trend within the field. The results obtained from the compaction trend analysis method reveal that overpressures in this field are associated with simple roll-over structures bounded by normal faults, and are caused mainly by undercompaction of Akata shale. The depth to top of mild overpressures (<0.71 psi/ft) in this field ranges from 8,000 to 11,000 ft. Similarly, the depth to top of severe overpressures (>7.10 psi/ft) ranges from about 12,000 to over 13,000 ft. Post-depositional faulting is believed to have controlled the configuration of the overpressure surface and has played later roles in modifying the present day depth to top of overpressures. Abnormal pressure trend within this field is observed to be trending towards the N–E direction.

Keywords Overpressure · Overburden gradient · Density · Resistivity · D-Exponent

S. A. Ugwu
Department of Geology, University of Port Harcourt, Port Harcourt, Nigeria
e-mail: ugwusa@yahoo.com

C. N. Nwankwo (✉)
Department of Physics, University of Port Harcourt, Port Harcourt, Nigeria
e-mail: cyrilnn@yahoo.com

Introduction

The pore spaces of sedimentary rocks below the water table filled with fluids of varying salinities are normally linked through interconnected network of pores, to pore fluids at the surface. Thus, the pressure of the pore fluids at depth is due to a continuous column of fluids which extends to the surface. This pressure invariably is a function of column height and the density of the fluids. The pore pressure exerted by one foot high column of fresh water and very saline water are 0.433 and 0.47 psi/ft and their densities are 1.0 and 1.09 g/cm^3, respectively. Fluid pressure gradient outside the range of 0.433–0.47 psi/ft in sedimentary sequence is termed abnormal.

Factors that enhance the formation of abnormally high pressure include the development of high shale to sand ratio, rapid sedimentary deposition, tectonic influences, aquathermal pressuring, osmosis and so on (Mouchet and Mitchel 1989). The unique characteristics of abnormal pressure zone are the development of abnormal porosities in shale sections, leading to abnormal pore fluid content.

Logging devices that give clue to this abnormal porosity development include sonic, resistivity and density. In addition to these logs (obtained after drilling), measurements are made during drilling operations that enable overpressured zones to be delineated. Such measurements include rate of penetration and drilling exponent, mud weight, gases, cuttings shape and size, torque and drag, etc. (Moutchet and Mitchel 1989).

Explorationists' interest in the Niger Delta has moved to mainly deep prospects onshore and deep/ultra deep prospects offshore. The deep campaign in the Niger Delta has demonstrated the need for a detailed overpressure and trap integrity analysis as an integral and required step in the prospect appraisal. This is because different trapping

scenarios can occur in which hydrocarbons are entirely lacking in a structure or are contained in a single or multi-phase in the respective hydropressured and overpressured sections. Similarly, the risk of dry or gas-charged traps increases with depth and overpressure magnitude in such situation also increases. For instance, it was observed that only two out of nine deep exploratory wells drilled by Nigeria Agip Oil Company between 1970 and 2005 were normally pressured (Nwaufa et al. 2006). In most of these cases, the wells were either abandoned, drilled without reaching the desired objective sequence, or drilling prolonged leading to astronomical rise in drilling cost. These problems were encountered despite the fact that the latest drilling practices were applied to most of the wells (Nwaufa et al. 2006).

Safe exploration of these deep prospects, therefore, would largely depend on our ability to understand the controls on top seal strength, overpressure generations/distributions, and trap integrity, and then confidently incorporate this knowledge into prospects evaluation and well designs. This is very important considering that in the current campaign for deeper prospects, the economic consequences of exploitation in areas with an unspecified risk of abnormal pressure profiles may range from increased drilling costs due to hazards to unrealized prospect potentials.

Overpressured formation exhibits several properties when compared with a normally pressured section at the same depth; including higher porosities, lower bulk densities, lower effective stress, higher temperature, lower interval velocities and higher Poisson's ratio. Well data measures some of these properties, which can be used to determine overpressure. Also, seismic interval velocities get influenced by changes in each of the above properties, and this is exhibited in terms of reflection amplitudes in seismic surveys. Consequently, velocity determination is the key to pore pressure prediction.

This study is aimed at predicting post-drill pore pressures in X-field, Onshore Niger Delta Basin using an integrated approach of pore pressure indicators from wireline logs, mudlogs, and qualitative/semi-quantitative data available in the real time which will enable overpressured zone to be delineated to a very close approximation. More so, the utilization of compaction-based techniques in predicting overpressure will give clue to the origin of overpressure in the Niger Delta region; formation pore pressure at the given depth will be calculated.

Location of the study area

The Well names are informal names given to the three wells operated by Nigerian Agip Oil Company (NAOC), in the eastern Niger Delta. The Oil Mining Lease (OML) was not indicated because of the understanding reached between the researcher and the company before the data were made available. The coordinates of the well locations were given as follows: WELL A (363:500N; 94:100E), WELLB (363:000N; 93:500E), WELLC (363:100N; 92:500E). This is shown in Fig. 1.

Geology and morphology of the study area

The onshore portion of the Niger Delta province is delineated by the geology of the southern Niger and southern–western Cameroon. The northern boundary is the Benin flank, an east northern trend hinge line south of the West African basement massif. The north–eastern boundary is defined by outcrops of the Cretaceous of the Abakaliki high and further east–southeast by the Calabar flank—a hinge line bordering the adjacent Precambrian. The offshore province of the region is defined by the Cameroon volcanic line to the east, the eastern boundary of the Dahomey Basin (the eastern–most western African passive margin) to the west, and the 2 km sediment thickness south and southwest. The province covers 300,000 km^2 and includes the geologic extent of the Tertiary Niger Delta (Akata-Agbada) petroleum system.

The fracture zone ridges in the deep Atlantic form the boundary faults of the Cretaceous Benue-Abakaliki trough, which cuts far into the West African shield. The trough represents a failed arm of a rift triple junction associated with the opening of the South Atlantic. In the region of the Niger Delta, rifting diminished altogether in the Late Cretaceous, giving rise to gravity tectonism deformational process. Figure 2 shows the gross paleogeography of the region as well as the relative position of the African and South American plates since rifting began.

The morphology of Niger Delta changed from an early stage spanning the Paleocene to early Eocene to a later stage of delta development in Miocene time. Delta progradation occurred along two major axes, the first paralleled the Niger River, where sediment supply exceeded subsidence rate. The second, smaller than the first, became active during Eocene to early Oligocene basin ward of the Cross River where shorelines advanced into the Olumbe-1 area (Short and Stauble 1967). This axis of deposition was separated from the main Niger Delta deposits by the Ihuo Embayment, which was later rapidly filled by advancing deposits of the Cross River and other local rivers (Short and Stauble 1967).

Stratigraphically, the Tertiary section of the Niger Delta is divided into three formations, representing prograding depositional facies that are distinguished mostly on the basis of sand–shale ratios. The type sections of these

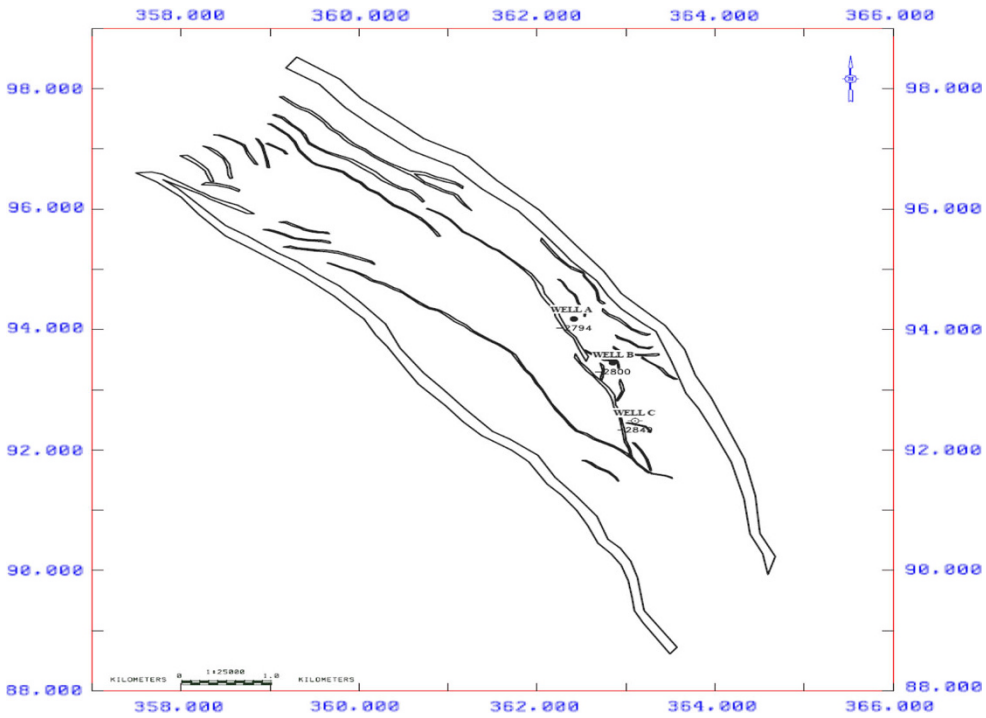

Fig. 1 Base map of location, showing the structural features of the field and the well positions

formations are described in Short and Stauble (1967) and summarized in a variety of papers (Avbovbo 1978; Doust and Omatshola 1990; Whiteman 1982; Evamy et al. 1978; Kulke 1995). They are the basal Paleocene to recent prodeltaic facies of the Akata Formation, the Eocene to recent, parallic facies of the Agbada Formation, and the Oligocene to recent, fluvial facies of the Benin Formation (Fig. 3). These lithostratigraphic units decrease in age basin ward, reflecting the overall regression of depositional environments within the Niger Delta clastic wedge. The formations reflect a gross coarsening-upward progradational clastic wedge (Short and Stauble 1967), deposited in marine, deltaic, and fluvial environments (Weber and Daukoru 1975).

Methodology

The data utilized in this project include drilling parameters, mudlog parameters and electrical/acoustic log parameters. Based on the available data, this study is limited to overpressure prediction methods while drilling and after drilling.

Method used while drilling

The D-exponent, shale density, rate of penetration (ROP), MWD Logs and qualitative pressure evaluation methods were applied. The most reliable detection technique is, however, the direct pressure-measuring tests which include kicks, formation interval tests (FIT), repeat formation tests (RFT), drill stem tests (DST), and production tests. All these tests are costly and demand for more stringent interpretation.

Method used after drilling (post-drilling)

Changes in pore pressure can be recognized on regular formation evaluation tools such as sonic, resistivity, neutron and density logs. The logs show the effect of pore pressure because of the relationship between compaction, porosity, density and the electrical and acoustic properties of the sediments. As rock compacts, the porosity is reduced and the density is increased, which also causes the bulk modulus and shear modulus to also increase because of increase in grain contact area and grain contact stress.

Overburden gradient calculation

Quantitative determination of pore pressure from wireline logs requires prior calculation of the overburden pressure. Overburden pressure is the pressure exerted by the weight of all the overlying sediments. The decrease in sediment porosity under the effect of burial (compaction) is proportional to the increase in overburden pressure. Overburden pressure gradient in psi/ft is a function of formation density (ρ) in g/cc × 0.434. Formation density varies with depth, so overburden pressure is a variable function of depth.

Formation density was estimated from acoustic travel time responses using Wylie's equation (1). The measurements are averaged over 500 m interval.

$$\rho_b = 0.64\,((1 - v/6489.36)/(1 + v/1525)) \quad (1)$$

where v is the acoustic velocity. A maximum matrix density p_{max}, value of 2.75 (g/cm^3) and fluid p_{fluid} value of 1.03 (g/cm^3) were used in the porosity computation.

The interval overburden in psi was calculated using the expression

$$s = 0.434 \times p \times \Delta h \quad (2)$$

where s is interval overburden pressure in Psi, Δh is the formation interval thickness (ft), p is density (g/cc), 0.434 is conversion factor that converts g/cc to psi/ft

The overburden pressure gradient was then determined from Eq. 3

$$S = \sum s / \sum h \times 0.052 \quad (3)$$

where S is overburden pressure gradient in psi/ft, $\sum s$ is cumulative interval overburden pressure in psi, $\sum h$ is cumulative interval thickness

The Mud Weight or Equivalent Mud Weight (ECD) is converted as follows as follows

$$\text{MW} = (\text{psi/ft}) / 0.052 \quad (4)$$

This is tabulated for the interval of interest (500 m and above) of the wells. The cumulative overburden is then plotted against TVD (true vertical depth) on a Cartesian coordinate as lithostatic pressure.

Shale resistivity method

The shale resistivity pore pressure technique is based on the principle that as normal compaction proceeds, pore water is progressively squeezed from shale (dewatering) and the shale becomes more compact and dense with increasing depth. Thus, they become more resistive with depth. A plot of shale resistivity versus depth for a basin of normally compacted shale will exhibit a trend of an even-increasing resistivity. Should the normal compaction process be interrupted or adversely influenced by such factors as restricted vertical/horizontal permeability, rapid rate of deposition, high shale/sand ratios, etc., and the normal rate of dewatering will be hindered. This results to abnormal pressure. The high fluid content in abnormally pressured shale is identifiable by a trend of decreasing resistivity with depth. Shale thickness of about 10–15 m was chosen and their depths noted.

All resistivity values which fall on the trendline are representative of normal pore pressure. Shale resistivity values which fall to the left of the trendline represent abnormally pressured shale, and when it points to the right of the trendlines, it represents cemented or contaminated shales. The normal compaction trendline is later extrapolated to cover area of interest. Pore pressure is quantified using Eaton's (1969) ratio equation for resistivity method:

$$P = S - \left((S - P_n)(R_o/R_n)^{1.2}\right) \quad (5)$$

where P is formation pore pressure, S is overburden pressure, P_n is Normal pore pressure (normally 0.433–0.464 psi/ft for Niger Delta Basin), R_o is observed resistivity at zone of interest, R_n is normal resistivity at zone of interest.

Shale transit time method

Sonic transit time is the measure of the time it takes a sound wave to travel one foot into the formation. This technique is applicable primarily for abnormal pressures which have been generated by compaction-related processes. The technique involves plotting shale transit times versus depth on semi-log paper. Plots of shale transit time versus depth will yield a steadily decreasing trend, since as density increases the time it takes for a sound wave to travel one foot decreases. As with resistivity method, a normal compaction trendline is established and it is extrapolated to areas of interest. Formation pore pressure was calculated using Eaton's ratio for shale transit time method.

$$P = S - \left((S - P_n)/(\Delta t_n/\Delta t_o)^{3.0}\right) \quad (6)$$

where P is formation pore pressure, S is overburden pressure, P_n is Normal pore pressure, Δt_n is normal sonic transit time, Δt_o is observed shale sonic transit time

Shale bulk density method

As compaction proceeds in a normal fashion, the density of the shale will increase with depth, therefore porosity (or pore fluid) will decrease. A plot of shale density versus depth indicates that bulk density increases with depth until overpressured zone is reached. If compaction is affected, the result is an increase in pore spaces and a corresponding decrease in density.

A normal compaction trendline is drawn across the normally pressured zone. Shale densities which are lower than the normal compaction trendline indicate abnormally pressured shale. Although there is a general trend, the spread of the data indicates that these measurements are not as reliable as the shale resistivity and sonic transit time evaluation. This is due to the fact that density logs are frequently affected by factors other than lithology, porosity and hydrocarbons (particularly gas). For this reason

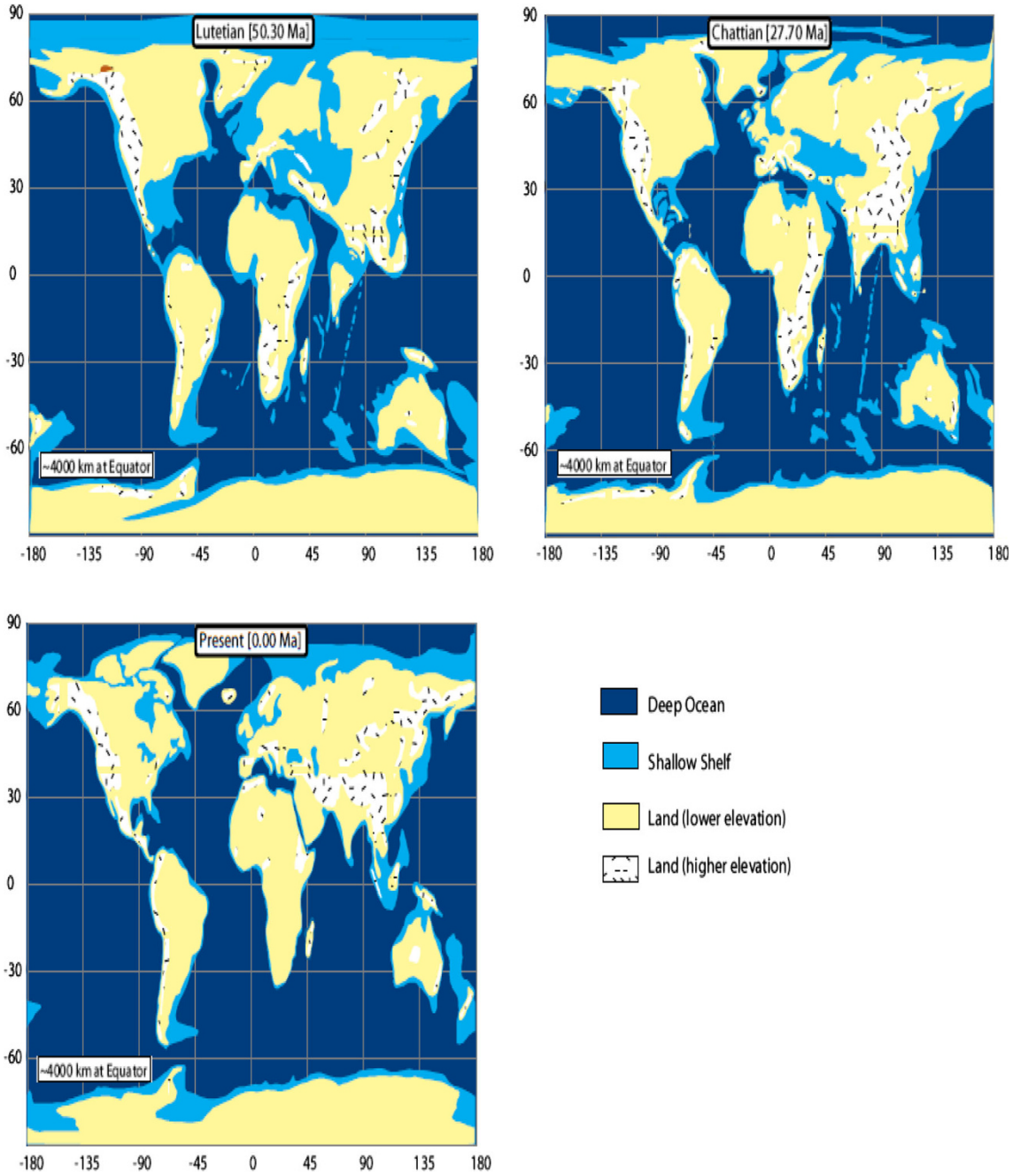

Fig. 2 The gross paleogeography of the region as well as the relative position of the African and South American plates since rifting began

emphasis was not placed on quantifying formation pressure from this technique but rather in delineating the onset of overpressure.

D-exponent method

The D-exponent is a mathematical expression which relates rate of penetration, rotary speed, bit size and bit weight to the effect of differential pressure. This is expressed as:

$$D = \left(\log(R/60\,\mathrm{N})/\log\left(12\,\mathrm{W}/10^6\,\mathrm{D}\right)\right) \quad (7)$$

where R is rate of penetration in (ft/h), N is rotary speed (in rev/h), W is weight on bit (in tons) D is bit size (inches)

For normally pressured sediments, the D-exponent yields a trend of increasing values with depth; a trend of decreasing values is often indicative of increasing pore pressure. If so interpreted, and if plotted, the difference between observed and normal values of d-exponent represent the magnitude of the pore pressure (Fig. 4). The D-

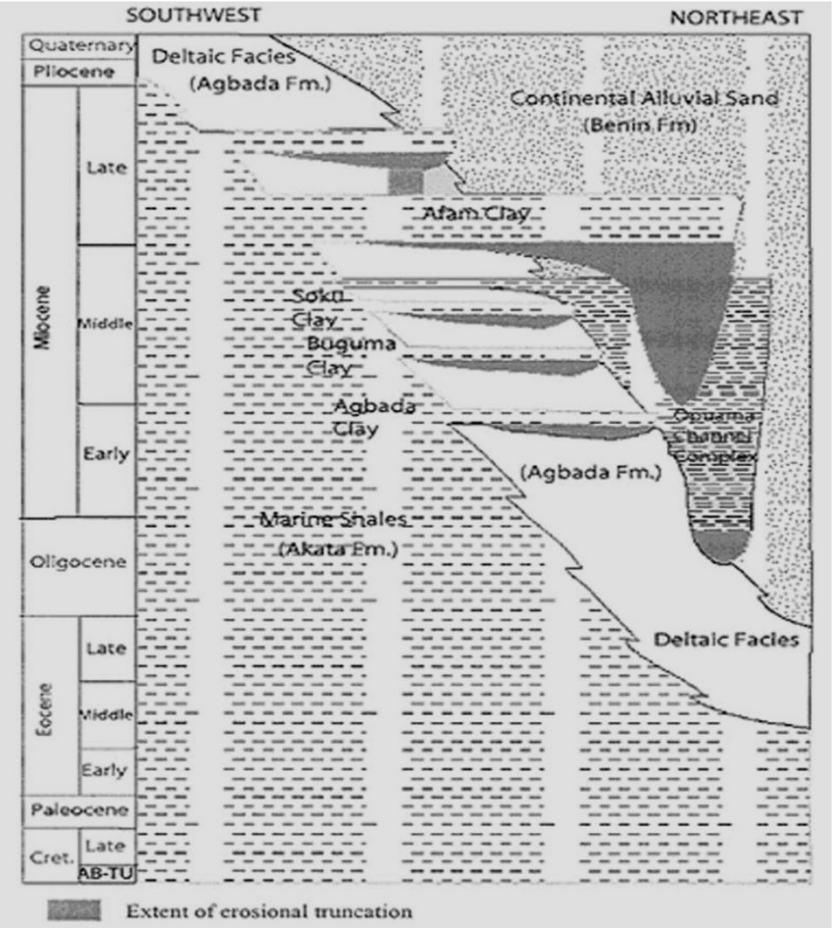

Fig. 3 Stratigraphic column showing formations of the Niger Delta

exponent may be corrected and normalized for changes in mud weight and/or ECD (equivalent circulating density) by the following:

$$\mathrm{Dc} = (\mathrm{d} \times \mathrm{normal\,pressure\,in\,ppg} / \mathrm{mud\,weight\,or\,ECD\,in\,ppg}) \quad (8)$$

Pore pressures can be estimated by utilizing various methods. One of these methods is by applying Eaton's formula as follows:

$$P = S - \left((S - P_{\mathrm{n}}) \left((d_{\mathrm{o}}/d_{\mathrm{n}})^{1.2} \right) \right) \quad (9)$$

where P is formation pore pressure of interest, P_{n} is normal pore pressure (for Niger Delta is 0.433–0.465 psi/ft), S is overburden pressure, d_{o} is observed d-exponent at the depth of interest, d_{n} is normal d-exponent at the depth of interest.

It may also be calculated using the following simple formula:

$$P = N \times d_{\mathrm{n}}/d_{\mathrm{o}} \quad (10)$$

where P is pore pressure in ppg, N is normal pore pressure in ppg, d_{n} is normal d-exponent, d_{o} is observed d-exponent

Results

Knowledge of the overburden pressure at each point in the well (described by the overburden gradient, S) is essential for formation pressure calculations. Cumulative overburden pressure gradient derived for the three wells, respectively, was utilized to estimate the pore pressure regime of the Field.

Figure 4 shows the trend of pore pressure indicators for real-time mudlog data. The pore pressure indicators include the D-exponent and mud weight. The plot shows that D-exp increases with depth until the top of overpressure is reached, at which it starts to decrease with increasing depth. The mud weight remains constantly steady until the top of overpressure is reached; below this depth, the mud weight increases continuously. The formation plot shows the various lithologies encountered. From the trends of the composite plot, the various formations can be delineated (change in formation such as Benin Formation to Agbada Formation). For the ease to estimate the formation pressures with depth, the key parameters were re-plotted singly (Fig. 5). Formation pressure estimated from D-exponent for Well B and Well C is tabulated as shown in Table 1.

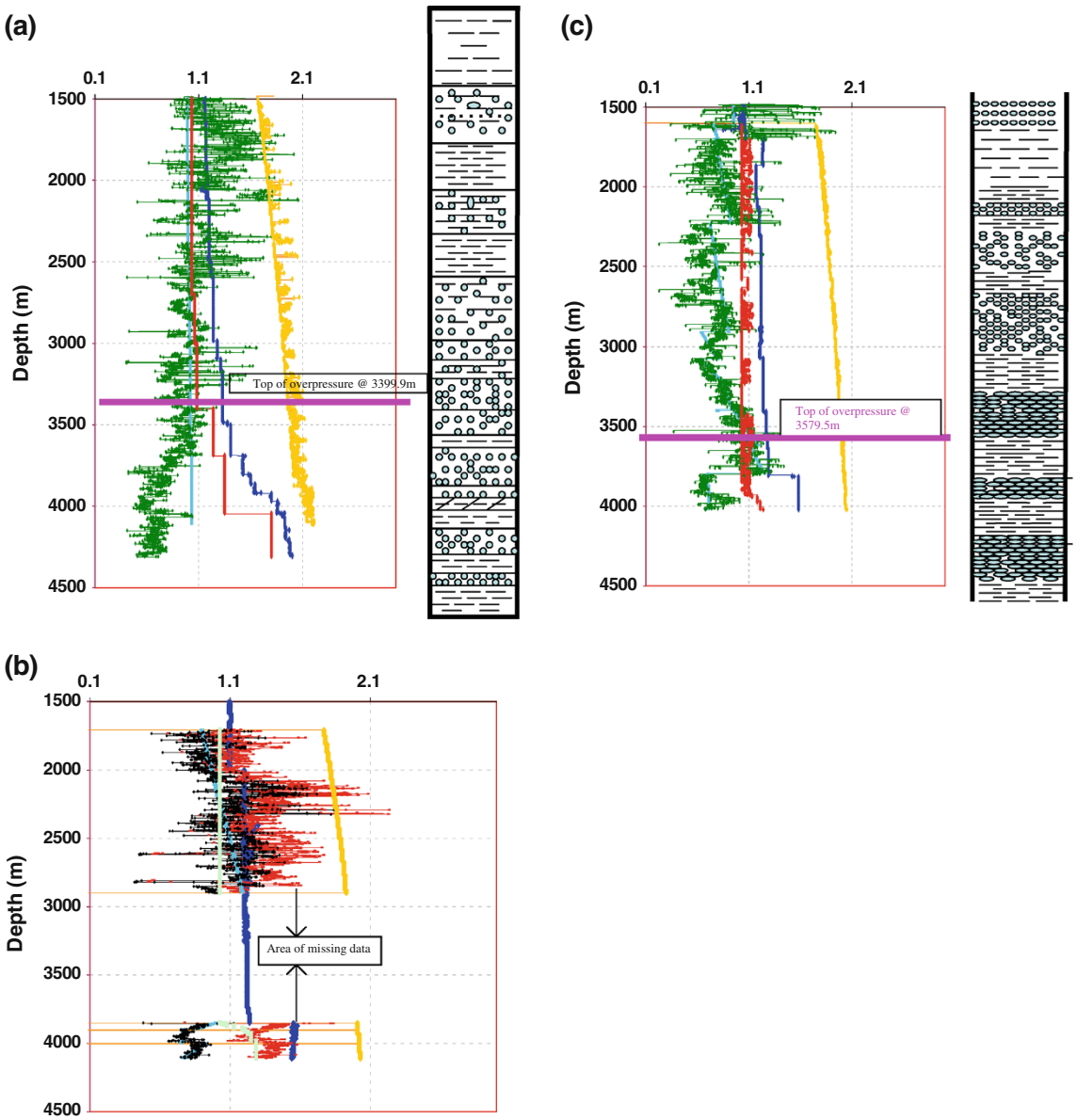

Fig. 4 **a** Composite plot for mudlog data for Well C, showing trends and behavior of the data KEYS: *green line* is d-expo, *redline* is formation pressure, *dark blue line* is mud weightout, *yellow line* is fracture pressure, *light blue line* is d-exp trend. **b** Composite plot for mudlog data for well A, showing trends and behavior of the data. KEYS: *green line* is d-expo, *red line* is formation pressure, *dark blue line* is mud weightout, *yellow line* is fracture pressure, *light blue line* is d-exp trend line. **c** Composite plot from mudlog data for Well B, show trends and behaviors of data KEYS: *green line* is d-expo, *red line* is formation pressure, *dark blue line* is mud weightout, *yellow line* is fracture pressure, *light blue line* is d-exp trend line

The plots from wireline data, which have its pore pressure indicators estimated mainly from resistivity and acoustic traveltime logs show that resistivity increases with depth and formation, until the top of overpressure is reached; below this depth, the resistivity tends to decrease. For acoustic waves, there is a consistency in the trend, until the top of overpressure is reached, at which the acoustic trend tends to show a slight increase (Fig. 6; Table 2).

A plot of the estimated pore pressure, hydrostatic pore pressure (Normal) and lithostatic pressure (overburden) versus depth mud and wireline data is presented in Figs. 7 and 8, respectively.

A plot of the estimated pore pressure, hydrostatic pore pressure (Normal) and lithostatic pressure (overburden) versus depth was presented from which the onset of overpressure can be identified.

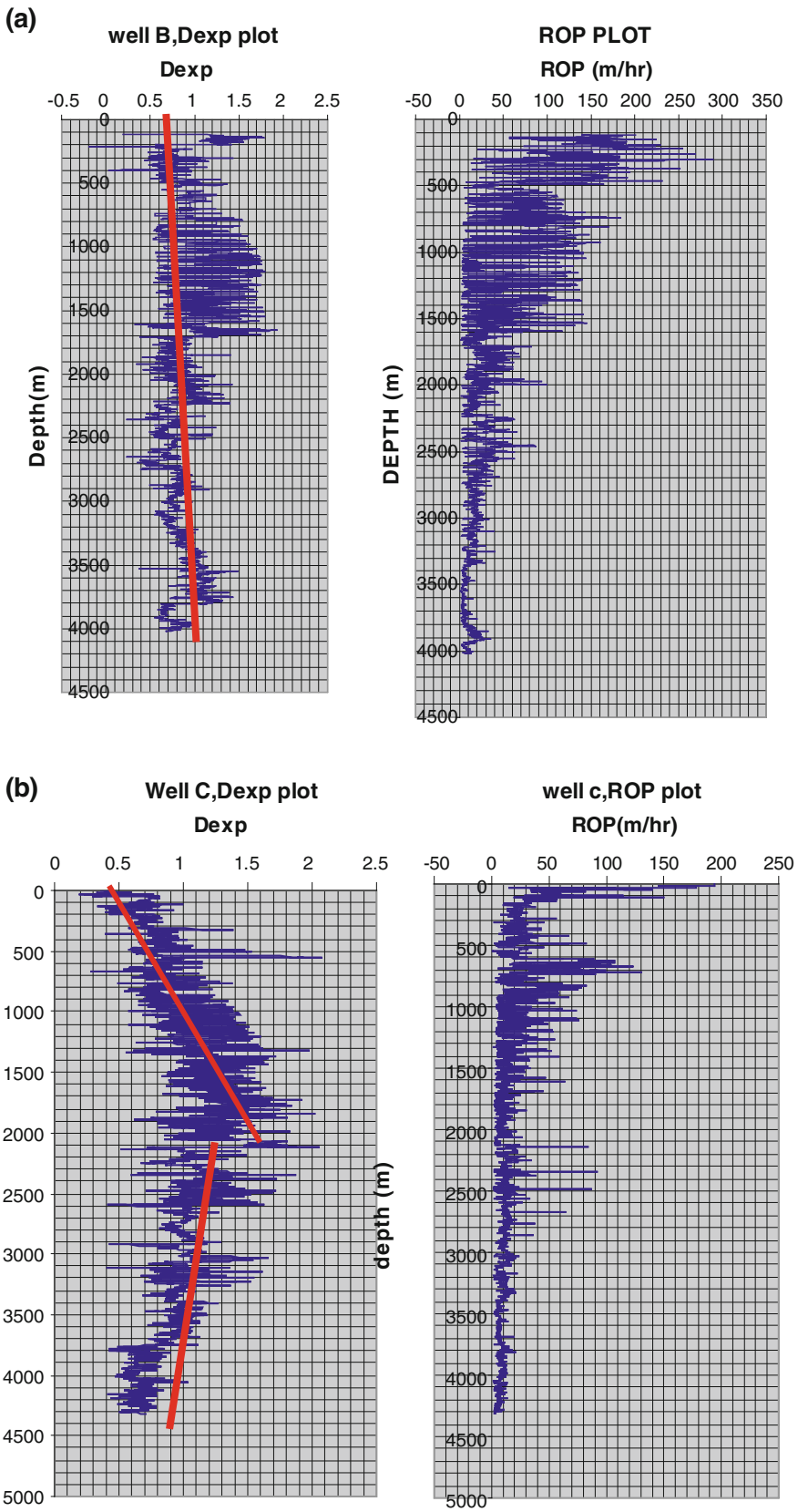

Fig. 5 **a** Re-plots of pore pressure indicators from well data (Dexp and Rop) for Well B. **b** Re-plots of pore pressure indicators from well data (Dexp and Rop) for Well C

Table 1 a Calculated pore pressure from D-exponent from Well B. b Calculated pore pressure from D-exponent from Well C

Depth (m)	Depth (ft)	Hydr Press Psi	Est Pore Press Psi	Est Pore Pres Gra Psi/ft	Est Pore Pres Gra ppg
a Calculated pore pressure from D-exponent from Well B					
500	1,641	763	721	0.4397	8.45
1,000	3,281	1,525	1,073	0.3272	6.29
1,500	4,922	2,288	1,923	0.3908	7.51
2,000	6,562	3,051	2,800	0.4268	8.2
2,500	8,203	3,814	3,986	0.486	9.34
2,600	8,531	3,966	3,953	0.4634	8.91
2,700	8,859	4,119	3,851	0.4348	8.36
2,800	9,187	4,271	3,965	0.4316	8.3
2,900	9,515	4,424	4,802	0.5047	9.7
3,000	9,843	4,576	5,159	0.5242	10.08
3,100	10,171	4,729	5,476	0.5384	10.35
3,200	10,499	4,882	6,177	0.5884	11.31
3,300	10,827	5,034	5,052	0.4667	8.97
3,400	11,155	5,187	4,600	0.4124	7.93
3,500	11,484	5,340	6,716	0.5849	11.24
3,600	11,812	5,492	5,918	0.5011	9.63
3,700	12,140	5,645	7,593	0.6255	12.02
3,800	12,468	5,797	9,574	0.7679	14.76
3,900	12,796	5,950	10,350	0.8089	15.55
4,000	13,124	6,102	11,282	0.8597	16.53
b Calculated pore pressure from D-exponent from Well C					
500	1,640	763	552	0.3366	6.47
1,000	3,281	1,526	902	0.2748	5.28
1,500	4,921	2,288	1,946	0.3954	7.6
2,000	6,562	3,051	1,648	0.2511	4.48
2,100	6,890	3,204	1,618	0.2348	4.52
2,200	7,218	3,356	3,870	0.5362	10.31
2,300	7,546	3,509	4,430	0.587	11.29
2,400	7,874	3,661	4,592	0.5832	11.22
2,500	8,202	3,814	2,665	0.3249	6.25
2,600	8,530	3,966	4,312	0.5055	9.72
2,700	8,858	4,119	4,762	0.5376	10.34
2,800	9,186	4,271	5,236	0.57	10.96
2,900	9,514	4,424	4,506	0.4736	9.1
3,000	9,843	4,577	3,096	0.3145	6.04
3,100	10,171	4,730	4,194	0.4123	7.93
3,200	10,499	4,882	4,612	0.4393	8.45
3,300	10,827	5,035	5,252	0.4851	9.33
3,400	11,155	5,187	6,062	0.5397	10.38
3,500	11,483	5,340	7,766	0.6763	13.38
3,600	11,811	5,492	8,402	0.7114	13.01
3,700	12,139	5,645	8,540	0.7035	13.58
3,800	12,467	5,797	10,316	0.8275	15.91
3,900	12,795	5,950	10,588	0.8275	15.91
4,000	13,124	6,103	11,057	0.8425	16.2

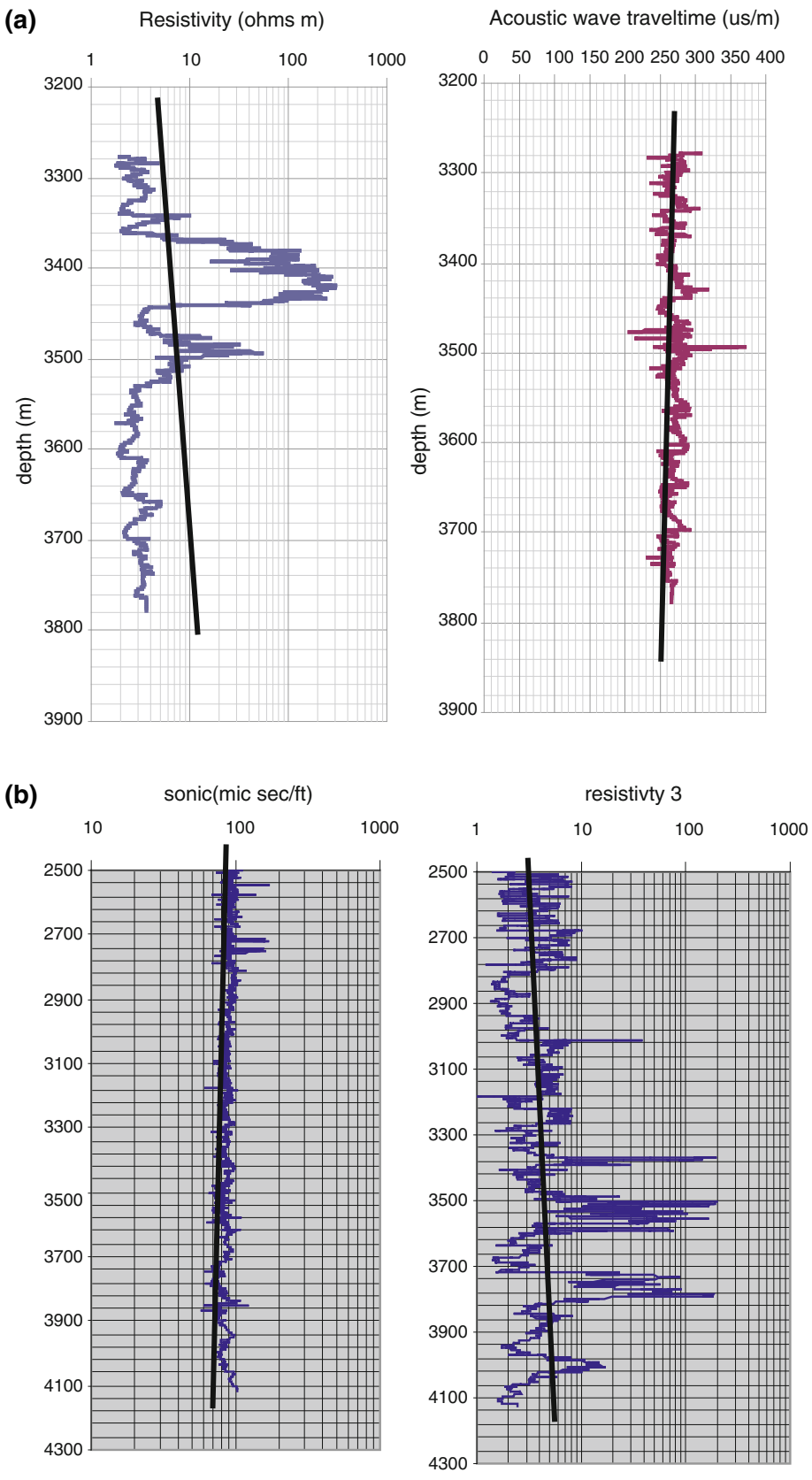

Fig. 6 **a** Re-plot of pore pressure indicators from wireline data for Well B. **b** Re-plot of pore pressure indicators from wireline data for well A

Table 2 a Estimated pore pressure from resistivity data for Well A. b Estimated pore pressure from sonic data for Well A. c Estimated pore pressure from sonic data for Well B. d Estimated pore pressure from resistivity data for Well B. e Estimated pore pressure from resistivity for Well C

Depth (m)	Depth (ft)	Hydr Press Psi	Est Pore Press Psi	Est Pore Pres Gra Psi/ft	Est Pore Pres Gra ppg
a Estimated pore pressure from resistivity data for Well A					
2,500	8,202	3,814.2	3,266.2	0.3982	7.65
2,550	8,366	3,890.4	2,955	0.3532	6.79
2,600	8,530	3,966.7	2,800.5	0.3283	6.31
2,650	8,694	4,043	3,144.8	0.3617	6.95
2,700	8,858	4,119.2	3,292.7	0.3717	7.14
2,750	9,022	4,195.5	3,953.7	0.4382	8.43
2,800	9,186	4,271.8	5,417.4	0.5897	11.34
2,850	9,350.8	4,348.1	5,649.6	0.6042	11.61
2,900	9,541.9	4,424.4	7,200.8	0.7568	14.55
2,950	9,678.9	4,500.7	6,299	0.6508	12.51
3,000	9,843	4,576.9	4,225.5	0.4293	8.25
3,050	10,007	4,653.3	3,734.6	0.3732	7.17
3,100	10,171	4,729.6	4,877.1	0.4795	9.22
3,150	10,335.2	4,805.8	5,204.7	0.5036	9.68
3,200	10,499	4,882.1	7,920.5	0.7544	14.5
3,250	10,663	4,958.4	6,965.2	0.6532	12.56
3,300	10,827	5,034.6	7,129.7	0.6585	12.66
3,350	10,991	5,110.9	7,505.9	0.6829	13.13
3,400	11,155	5,187.2	7,309	0.6552	12.6
3,450	11,319	5,263.5	6,643.3	0.5869	11.28
3,500	11,483	5,339.8	6,178.1	0.538	10.34
3,550	11,647	5,416.1	6,683.3	0.5738	11.03
3,600	11,811	5,492.1	6,641.3	0.5623	10.81
3,640	11,942	5,553	7,904.4	0.6619	12.81
3,680	12,074	5,614.4	8,477.1	0.7021	13.5
3,720	12,205	5,675.3	7,132.6	0.5844	11.23
3,760	12,336	5,736.2	7,854.3	0.6367	12.24
3,800	12,467	5,797.1	8,144.6	0.6533	12.56
3,840	12,599	5,858.5	8,208.2	0.6515	12.52
3,880	12,730	5,919.4	8,963.1	0.7041	13.54
3,920	12,861	5,980.3	10,623.1	0.826	15.88
3,960	12,992	6,041.2	11,141.9	0.8576	16.49
4,000	13,124	6,102.6	11,463.8	0.8735	16.79
4,040	13,255	6,163.5	10,854.5	0.8189	15.74
4,080	13,386	6,224.4	11,720.7	0.8756	16.83
b Estimated pore pressure from sonic data for Well A					
2,500	8,202	3,814.1	3,434	0.4187	8.05
2,540	8,333	3,875.1	3,453	0.4143	7.96
2,580	8,464	3,936.1	3,962	0.468	9
2,620	8,596	3,997.8	4,287.8	0.4988	9.59
2,660	8,727	4,058	3,510.8	0.4023	7.73
2,700	8,858	4,119.2	5,159.3	0.5824	11.2
2,740	8,989	4,180.3	4,690.9	0.5218	10.03
2,780	9,121	4,241.3	4,221.3	0.4628	8.9
2,820	9,252	4,302.4	5,383.9	0.5819	11.19

Table 2 continued

Depth (m)	Depth (ft)	Hydr Press Psi	Est Pore Press Psi	Est Pore Pres Gra Psi/ft	Est Pore Pres Gra ppg
2,860	9,383	4,363.4	5,297.9	0.5646	10.85
2,900	9,514	4,424.4	4,702.3	0.4942	9.5
2,940	9,646	4,485.4	4,767.1	0.4942	9.5
2,980	9,777	4,546.5	3,729.1	0.3814	7.33
3,020	9,908	4,607.5	4,111	0.4149	7.97
3,060	10,039	4,668.5	4,099.3	0.4083	7.85
3,100	10,171	4,729.6	6,577.6	0.6467	12.43
3,140	10,302	4,790.6	6,712.8	0.6516	12.53
3,180	10,433	4,851.6	5,975.3	0.5727	11.01
3,220	10,564	4,912.6	6,463.5	0.6118	11.76
3,260	10,696	4,973.6	5,376.8	0.5027	9.66
3,300	10,827	5,034.7	6,139	0.567	10.9
3,340	10,958	5,095.7	6,032.6	0.5505	10.58
3,380	11,089	5,156.7	5,686.7	0.5128	9.86
3,420	11,221	5,217.7	7,173.5	0.6393	12.29
3,460	11,352	5,278.8	6,550.3	0.577	11.09
3,500	11,483	5,339.8	6,178.1	0.538	10.34
3,540	11,614	5,400.9	6,327.6	0.5448	10.47
3,580	11,745	5,461.8	6,408.5	0.5456	10.49
3,600	11,811	5,492.1	6,442.9	0.5455	10.49
3,640	11,942	5,553	6,639.7	0.556	10.69
3,680	12,074	5,614.4	8,125.8	0.673	12.94
3,720	12,205	5,675.3	7,454.8	0.6108	11.74
3,760	12,336	5,736.2	7,733.4	0.6269	12.05
3,800	12,467	5,797.1	8,178.3	0.656	12.61
3,840	12,599	5,858.5	8,734.8	0.6933	13.33
3,880	12,730	5,919.4	8,069.5	0.6369	12.24
3,920	12,861	5,980.3	8,450.9	0.6571	12.63
3,960	12,992	6,041.2	10,267.5	0.7903	15.19
4,000	13,124	6,102.6	9,278.6	0.707	13.59
4,040	13,255	6,163.5	10,649	0.8034	15.45
4,080	13,386	6,224.4	11,744.8	0.8774	16.87
c Estimated pore pressure from sonic data for Well B					
3,300	10,827	5,034	5,524	0.5102	9.81
3,340	10,958	5,095	5,382	0.4912	9.44
3,380	11,089	5,156	3,763	0.3394	6.52
3,420	11,221	5,217	4,490	0.4002	7.69
3,460	11,352	5,278	5,080	0.4475	8.6
3,500	11,483	5,339	5,622	0.4896	9.41
3,540	11,614	5,400	6,542	0.5633	10.83
3,580	11,745	5,461	6,079	0.5176	9.95
3,620	11,877	5,522	7,265	0.6117	11.76
3,660	12,008	5,583	7,405	0.6167	11.85
3,700	12,139	5,644	8,431	0.6946	13.35
3,740	12,270	5,705	8,197	0.6681	12.84
3,780	12,402	5,766	8,744	0.7051	13.55

Table 2 continued

Depth (m)	Depth (ft)	Hydr Press Psi	Est Pore Press Psi	Est Pore Pres Gra Psi/ft	Est Pore Pres Gra ppg
d Estimated pore pressure from resistivity data for Well B					
3,300	10,827	5,035	5,876	0.5428	10.43
3,340	10,958	5,095	6,288	0.5739	11.03
3,380	11,089	5,156	3,420	0.3085	5.93
3,420	11,221	5,217	5,000	0.4456	8.57
3,460	11,352	5,278	5,339	0.4704	9.04
3,500	11,483	5,339	5,452	0.4748	9.13
3,540	11,614	5,400	7,277	0.6266	12.05
3,580	11,745	5,461	7,906	0.6732	12.94
3,620	11,877	5,522	8,406	0.7078	13.61
3,660	12,008	5,583	8,436	0.7026	13.51
3,700	12,139	5,644	8,498	0.7001	13.46
3,740	12,270	5,705	8,353	0.6,808	13.09
3,780	12,402	5,766	8,315	0.6705	12.89
e Estimated pore pressure from resistivity for Well C					
3,000	9,843	4,576	2,960	0.3008	5.78
3,040	9,974	4,637	3,671	0.3681	7.07
3,080	10,105	4,698	3,210	0.3177	6.1
3,120	10,236	4,759	3,791	0.3704	7.12
3,160	10,367	4,820	3,413	0.3293	6.33
3,200	10,499	4,882	1,460	0.1391	2.67
3,240	10,630	4,942	3,920	0.3688	7.09
3,280	10,761	5,003	2,420	0.2249	4.32
3,320	10,892	5,064	5,359	0.4921	9.46
3,360	11,024	5,126	4,622	0.4193	8.06
3,400	11,155	5,187	5,049	0.4527	8.7
3,440	11,286	5,247	6,598	0.5847	11.24
3,480	11,417	5,308	6,183	0.5416	10.41
3,500	11,483	5,340	6,250	0.5443	10.47
3,540	11,614	5,401	6,730	0.5795	11.14
3,580	11,745	5,461	6,962	0.5928	11.4
3,620	11,877	5,523	8,498	0.7155	13.76
3,660	12,008	5,584	9,303	0.7747	14.89
3,700	12,139	5,645	9,768	0.8047	15.48
3,740	12,270	5,706	10,809	0.8809	16.94
3,780	12,402	5,767	10,075	0.8124	15.62
3,820	12,533	5,828	10,806	0.8624	16.58
3,860	12,664	5,889	11,053	0.8728	16.78
3,900	12,795	5,950	10,116	0.7880	15.2
3,940	12,927	6,011	10,396	0.8461	15.47

Discussion of results

Detailed analysis of the mudlog data available in this study indicates that top of overpressure for Well A is at an average depth of 10,105 ft (3,079.8 m). Using the wireline data, the top of overpressure was estimated from sonic data at 10,039 ft (3,059.7 m) and from resistivity data at 10,171 ft (3,099.9 m). Below this depth, much of the overburden weight is borne by the pore fluids resulting to increase in pressure.

Calculated pore pressure within the zone of abnormal pressure development from sonic data is 0.655 psi/ft (6,577 psi) of mild pressure, to 0.8774 psi/ft (11,744.8 psi) of overpressure. Also, calculated pore pressure from

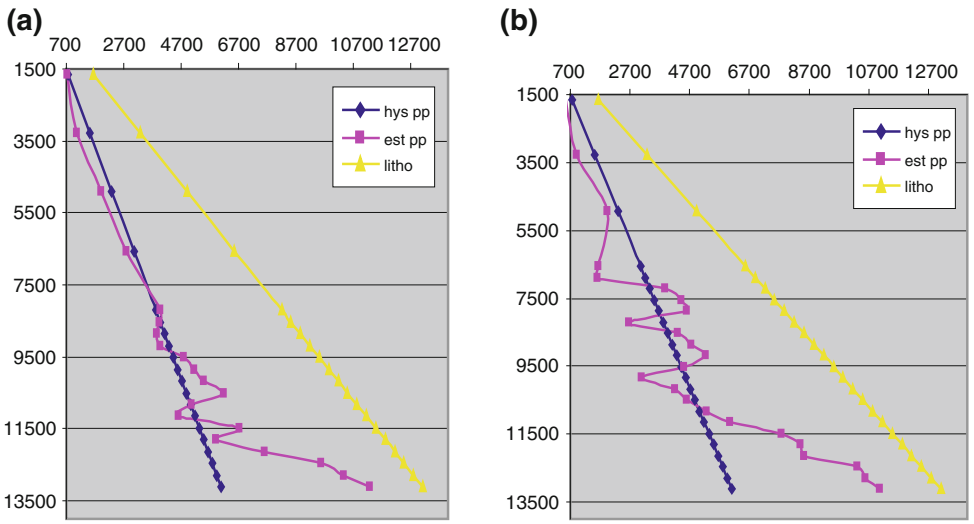

Fig. 7 **a** Estimated pore pressure for Well B, from D-exponent. **b** Estimated pore pressure for Well C, from D-exponent

resistivity data is 0.552 psi/ft (5,622 psi) of mild pressure, to 0.8756 psi/ft (11,720 psi) of overpressure. Below this depth (top of overpressure), the estimated pore pressure trend diverts from the hydrostatic (normal) pressure trend, increasing toward the lithostatic pressure (Fig. 8). This is due to the fact that the bulk volume is taken over by pore fluids resulting to decrease in resistivity data and slight increase in sonic data and also a decrease in bulk density. Much of the overburden weight is borne by the pore fluids, thus its pressure increased from normal 0.465 to 0.6467 psi/ft at 10,171 ft as shown in Table 2b. More so, the occurrence of about 85 % lithology of shale within this zone and an increase in the gas components and gas percentages are good indicators that abnormal pressure exist in this zone.

Opara and Onuoha (2009) stated that overpressures are mega-structurally and stratigraphically controlled, and vary from depobelts to depobelts within Niger Delta. The predicted top of overpressure as established by Ichara and Avbovbo (1985a, b) for Niger Delta is 13,000 ft (max value); also Opara and Onuoha (2009) revealed that the majority of the overpressure within the Niger Delta occurs between the depth interval of 6,000–13,000 ft, while that deduced from this study reveals that the onset of overpressure to hard pressure occurs between the depth interval of 10,000–12,650 ft of shale formation. This may be due to mud diaper, hydrocarbon generation and normal faults within the field, as can be seen on the base map.

Well B was drilled to a total depth (TD) of 4,020 m (13,189.6 ft). The Well kicked at a depth of 3,800 m (12,467.8 ft) and was killed with a mud weight of 13.2 ppg. Evaluation of the data available in this well shows that the top of overpressure is at an average depth of 11,373.6 ft (3,466.4 m). Using drilling exponent data, top of overpressure was at 11,155 ft (3,399.8 m) while using wireline data, the top established from Acoustic wave plot occurs at 11,483 ft (3,499.8 m). Also, from Resistivity plot, the overpressure occurs at 11,483 ft (3,499.8 m). Below this depth, much of the overburden weight is borne by the pore fluids resulting to pressure increase. Estimated pore pressure within the zone of abnormal pressure development from Acoustic wave traveltime ranges from a mild pressure of 0.5633 psi/ft (6,542 psi) to 0.7051 psi/ft (8,744 psi) of overpressure. Also, calculated pore pressures within Zone of abnormal pressure development from Resistivity are 0.6266 psi/ft (7,277 psi) of mild pressure to 0.7001 psi/ft (8,498 psi) of overpressure.

The calculated pore pressure from Well data (D-exponent) is 0.5633 psi/ft of mild pore pressure to 0.8397 psi/ft of overpressure. Below this depth (top of overpressure), the estimated pore pressure trend tends to divert from Hydrostatic (Normal) pressure, while increasing towards the lithostatic pressure. This is due to the fact that the bulk volume is taken over by pore fluids resulting to a decrease in resistivity, slight increase in Acoustic wave traveltime, decrease in bulk density and also a decrease in D-exponent. Comparing the pore pressure estimated from both well data (D-exponent) and wireline data show that the abnormal pressure are originating from the same range of depth (11,300–11,400 ft), with percentage lithology (close 100 % shale). The increase in gas component and the shale percentage lithology is a good indication that abnormal pressure exists.

Well C was drilled to a true vertical depth (TVD) of 4,309 m (14,137 ft). The well kicked at 4,050 m (13,288 ft) and was killed with a mud weight of 16.6 ppg. Informations from available data for this well explain that the top of overpressure is at an average depth of 10,991 ft (3,349.8 m). Using drilling exponent data, top of overpressure was at 11,155 ft (3,399.8 m), while that estimated from wireline, i.e., resistivity data, is at 11,286 ft

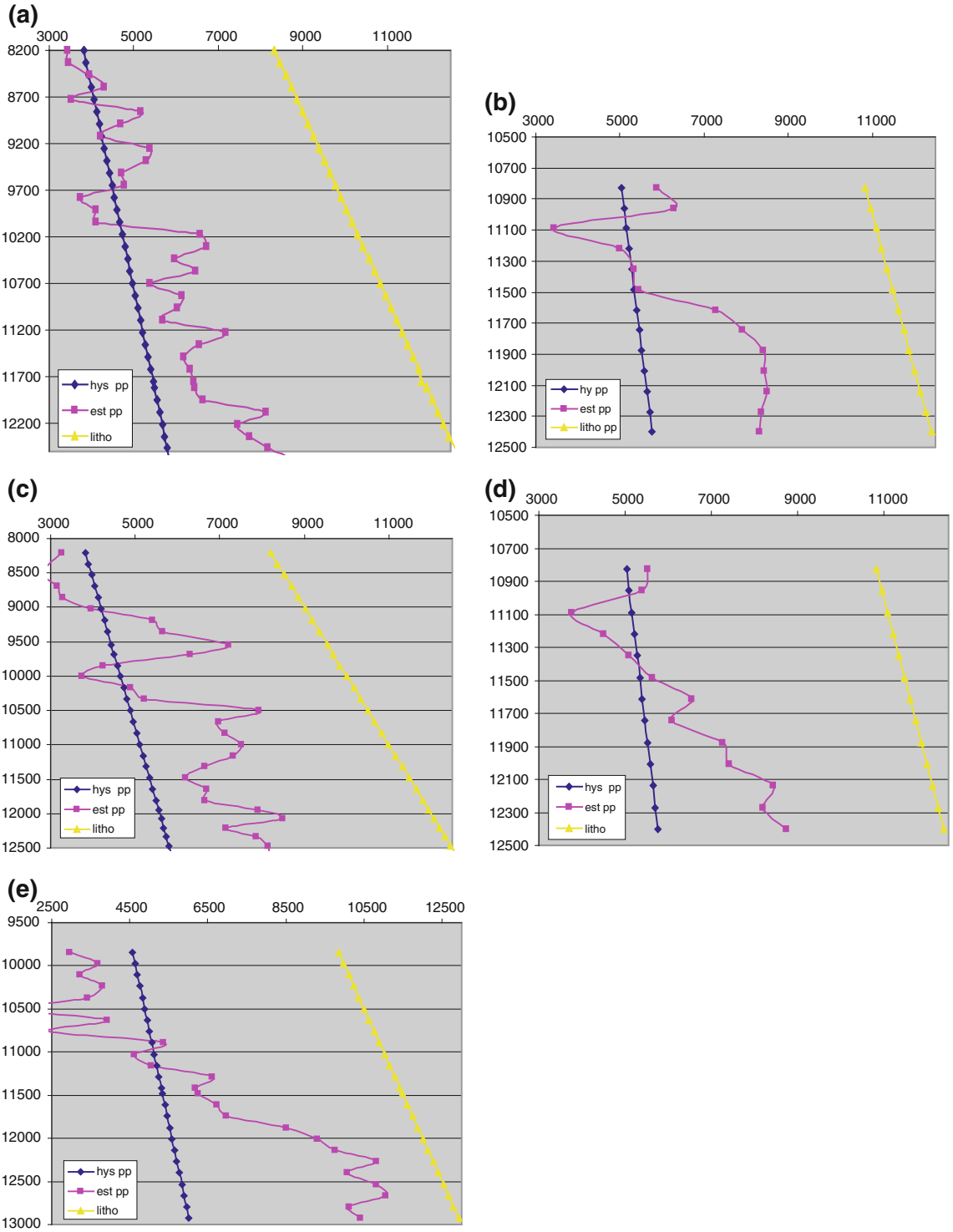

Fig. 8 **a** Estimated pore pressure trend for well A, from sonic. **b** Estimated pore pressure trend for well A, from resistivity. **c** Estimated pore pressure trend for Well B, from resistivity. **d** Estimated pore pressure for Well B, from acoustic-wave traveltime. **e** Estimated pore pressure for Well C, from resistivity

(3,440 m). Pore pressure determined within the zone of abnormal pressure development from resistivity data was 0.5847 psi/ft (10,396 psi).

The lithologies of the wells were generated and the tops of overpressure of the wells were correlated as shown in Fig. 9. This explains the trend of abnormal pressure with

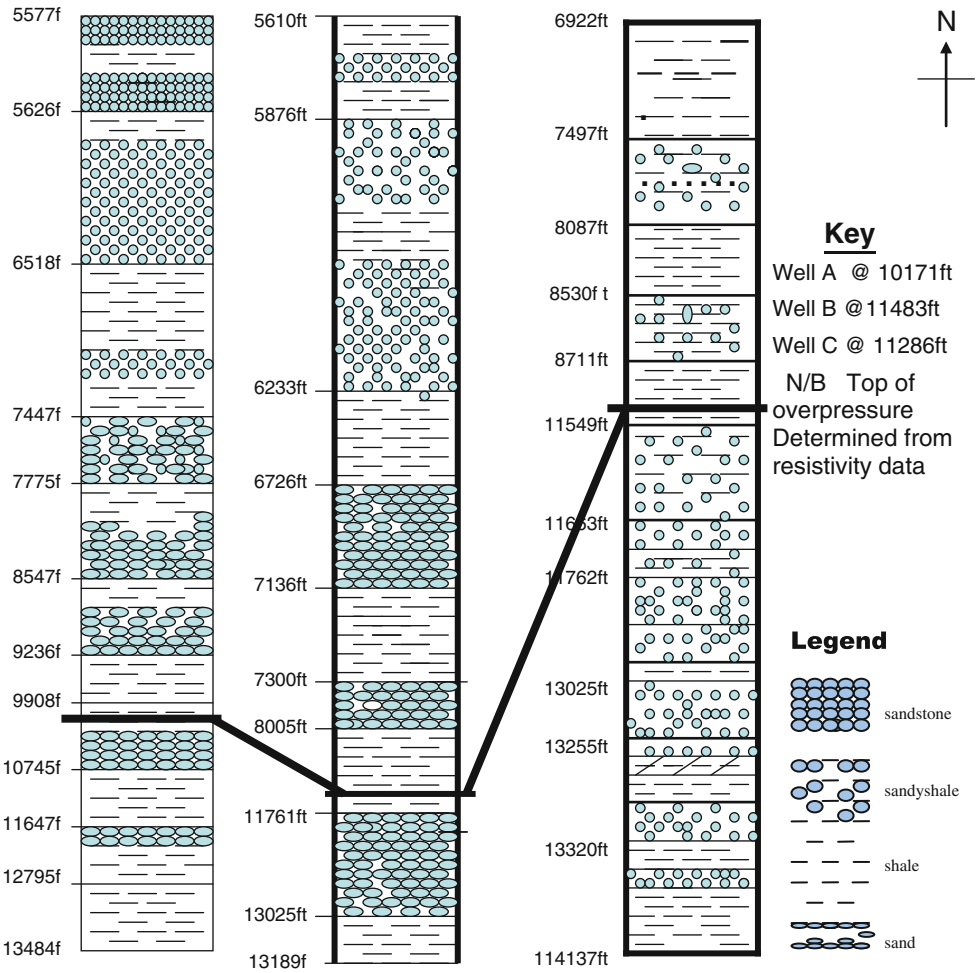

Fig. 9 Schematic correlation of overpressure with depth, which shows trend of overpressure across the field

depth within the field to be in the N–E direction. Equally, this shows that the top of abnormal pressure would be encountered at deeper depth, while drilling in this direction.

Pore pressure prediction and interpretation in X-field, Onshore Niger Delta basin revealed that the onset of mild pressure (<0.71 psi/ft) in the area to be about 11,745 ft (3,580 m) for Well B, 11,745 ft (3,580 m) for Well C and for Well A is at 10,171 ft (3,099.9 m). Analysis from both wireline and well data (mudlog) revealed that very high overpressure approaching lithostatic pressures are expected at deeper intervals between 13,000 ft and beyond. Distribution of overpressures shows a well-defined trend with depth to top of overpressures, increasing towards the central part of the field to a maximum depth of about 13,124 ft (4,000 m). This variation in the depth of top of overpressures within the area is believed to be related to Normal faulting and clay diapirism with top of overpressure becoming shallower with shale diapirism while moving towards the north direction of the field and deeper with sedimentation while moving towards the Northeast direction of the field as shown in the base map. Similarly, data acquired in deep wells from concessions in the Niger Delta show no micro-structural trend. Rather, overpressures were observed in the areas with normal fault pattern. It is most likely that these faults patterns have effect on the formation pressure, providing relief to potential pressure build-up (Nwaufa et al. 2006). Hanging wall closure is most often sealing and, therefore, retains significant columns of hydrocarbon, often leading to high minimum effective stress and fluid charging. Similarly, late hydrocarbon generation and shale diagenesis often lead to overpressure within upthrown shale (Evamy et al. 1978).

In addition, it was revealed that majority of the overpressure situation occurs between the depth of 10,000 ft (3,047.9 m) and 13,000 ft (3,962.2 m) falling largely within the Agbada Formation. In the Niger Delta basin, the occurrence of overpressures is largely believed to be associated with the undercompacted shales of the Akata Formation. However, previous studies by Ichara and Avbovbo 1978 and Weber and Daukoru 1975, have shown that overpressures in the Niger Delta usually occur shallower than Akata Formation. Explaining this phenomenon, Weber and Daukoru 1975 reveal that overpressures are

encountered in the Tertiary Niger Delta as a result of rapid loading of the undercompacted shales of Akata Formation by the sandy Agbada Formation and the Benin Formation. In each case, fluids expelled from the overpressured Akata Shales may inflate (charge) the pressures in the adjacent sands. Similarly, most of the mild overpressures within the Agbada Formation in the Niger Delta are as a result of the undercompaction (possibly chemical compaction disequilibrium) of the interbedded Marine Shales of the lower Agbada Formation. Consequently, overpressures are often encountered before the Akata Shales are reached.

Conclusion

It is concluded from this study that the X-field Onshore Niger Delta is overpresssured and the top of overpressure predicted from this research revealed the onset of mild pressure (<0.71 psi/ft) in the area to be about 10,000 ft of true vertical depth (TVD) while higher pressures (>0.71 psi/ft) were encountered at about 13,000 ft (TVD). The establishment of a clear compaction trend for all the wells indicates that undercompaction is the major cause of abnormal pressure in the field. It is observed that the abnormal pressure in this field tends to increase with depth in the N–E direction.

A combination of other factors such as Tectonic stress (Normal Faults), hydrocarbon generation, Clay diaphirs and Shale diagenesis, also contributed to the Abnormal pressure existing within this field. Also, the overpressure distribution in this field can be tied to that of the entire Niger Delta, which is said to be structurally and stratigraphically controlled.

Acknowledgments The Authors are grateful to Nigerian Agip Oil Company Port Harcourt for the provision of data used for this study and to Mr. C.A. Ihejieto for his all his contributions.

References

Avbovbo AA (1978) Geothermal gradients in the Southern Nigerian Basin. Bull Can Pet Geol 26:269–274

Doust H, Omatsola E (1990) Niger delta. In: Edwards JD, Santogrossi PA (eds) Divergent/passive margin basins. AAPG Mem 45:239–248

Eaton BA (1969) Fracture gradient prediction and its application in oilfield operation. J Pet Technol 21(10):1353–1360

Evamy BD, Harembourne J, Kamerling P, Knaap WA, Molley FA, Rowlands PH (1978) Hydrocarbon habitat of the Tertiary Niger Delta. AAPG Bull l62:1–39

Ichara MJ, Avbovbo AA (1985a) How to handle abnormal pressures in Nigeria's Niger Delta area. J Pet Technol 83(10):122–124

Ichara MJ, Avbovbo AA (1985) Study, to identify the Niger Delta Log parameters and VSP Trends. Oil Gas J 94–101

Kulke H (1995) Nigeria. In: Kulke H (ed) Regional petroleum geology of the world part 2; Africa, America, Australia and Antarctica, pp 143–172

Mouchet JP, Mitchele A (1989) Abnormal pressures while drilling-Origins, prediction, detection, evaluation. Manuals techniques 2, Elf Aquitane edition, Boussens, p 253

Nwaufa WA, Horsfall DE, Ojo CA (2006) Advances in deep drilling in the Niger Delta, 1970–2000. In: NAOC experience, NAPE conference proceedings, August 2006, pp 5–14

Opara AI, Onuoha KM (2009) Overpressure and trap integrity studies in parts of the Onshore, Niger Delta Basin: implications for hydrocarbon exploitation and prospectivity. SPE J 240–242

Short KC, Stauble AJ (1967) Outline of geology of the Niger Delta. AAPG Bull 51:761–779

Weber KJ, Daukoru EM (1975) Petroleum geology of the Niger Delta. World Pet Congr Proc 2:209–221

Whiteman AJ (1982) Nigeria, its petroleum geology, resources and potentials. Graham Trotman Lond 2:276–297